Sediment transport at the network scale and its link to channel morphology in the braided Vjosa River system

Simone Bizzi, Marco Tangi, Rafael Schmitt, John Pitlick, Hervé Piégay, Andrea Francesco Castelletti

Earth Surface Processes and Landforms

Sediment transport at the network scale and its link to channel morphology in the Vjosa River basin

Journal:	*Earth Surface Processes and Landforms*
Manuscript ID	Draft
Wiley - Manuscript type:	Research Article
Keywords:	sediment connectivity, network-scale sediment modeling, braided river, Balkan rivers, sediment transport, transport capacity

Abstract:

Recent years have seen an increase in sediment connectivity models to quantify fluxes, size, and provenances of sediment in river networks for improving pour understanding of fundamental processes and for informing river management.
Yet, the wide application of such models is still limited by a number of factors, uncertainty in model hypotheses, and the lack of data for model building and validation. To solve that challenge, we propose a novel approach to more robustly parameterize and validate network connectivity models.
We illustrate these points by applying the CASCADE sediment connectivity model to the Vjosa river in Albania. The Vjosa is one of the last unimpaired braided rivers in Europe and, at the same time, a data scarce environment. To initialize the model, we use remotely sensed data and modelled hydrology from a regional model. We perform a reach-by-reach optimization of surface grain size distribution (GSD) and thus transport capacity to ensure equilibrium conditions throughout the network. We then perform a sensitivity analysis, altering key parameters of the transport capacity calculation throughout the network, and compare results to surficial GSD from 6 reaches, channel morphology indicators, and observed values of total transport at the outlet. We then assess network-scale sensitivity to planform type shifts due to sediment starvation.
GSD and sediment fluxes generated by the sensitivity analysis have quantiles that match those observed in the field and reported in literature. Modelled thresholds for the transition between braided/non-braided reaches closely fit observations.
Those findings indicate that some basic assumptions, global data, and sediment transport equations can generate realistic representations of network scale sediment transport processes and the resulting river geomorphology. The proposed method is widely applicable and opens avenue for enabling widespread application of network-scale sediment connectivity models in river science and management while considering for ranges and drivers of uncertainty.

Sediment transport at the network scale and its link to channel morphology in the Vjosa River basin

S. Bizzi[1], M. Tangi[2], R. Schmitt[3], J. Pitlick[4], H. Piegay[5], A. Castelletti[2]

1 Department of Geosciences, University of Padova, Padua, Italy.

2 Department of Electronics, Information, and Bioengineering, Politecnico di Milano, Milano, Italy.

3 Natural Capital Project, Department of Biology and the Woods Institute for the Environment, Stanford University, Stanford, CA, USA

4 Department of Geography, University of Colorado, Boulder, Colorado, USA.

5 University of Lyon, CNRS-UMR 5600, Site of ENS Lyon, 15 Parvis René Descartes, F-69342, Lyon, France

ABSTRACT

Recent years have seen an increase in sediment connectivity models to quantify fluxes, size, and provenances of sediment in river networks for improving pour understanding of fundamental processes and for informing river management.

Yet, the wide application of such models is still limited by a number of factors, uncertainty in model hypotheses, and the lack of data for model building and validation. To solve that challenge, we propose a novel approach to more robustly parameterize and validate network connectivity models.

We illustrate these points by applying the CASCADE sediment connectivity model to the Vjosa river in Albania. The Vjosa is one of the last unimpaired braided rivers in Europe and, at the same time, a data scarce environment. To initialize the model, we use remotely sensed data and modelled hydrology from a regional model. We perform a reach-by-reach optimization of surface grain size distribution (GSD) and thus transport capacity to ensure equilibrium conditions throughout the network. We then perform a sensitivity analysis, altering key parameters of the transport capacity calculation throughout the network, and compare results to surficial GSD from 6 reaches, channel morphology indicators, and

observed values of total transport at the outlet. We then assess network-scale sensitivity to planform type shifts due to sediment starvation.

GSD and sediment fluxes generated by the sensitivity analysis have quantiles that match those observed in the field and reported in literature. Modelled thresholds for the transition between braided/non-braided reaches closely fit observations.

Those findings indicate that some basic assumptions, global data, and sediment transport equations can generate realistic representations of network scale sediment transport processes and the resulting river geomorphology. The proposed method is widely applicable and opens avenue for enabling widespread application of network-scale sediment connectivity models in river science and management while considering for ranges and drivers of uncertainty.

Keywords: sediment connectivity, network-scale sediment modeling, braided river, sediment transport, transport capacity, Balkan rivers.

INTRODUCTION

Understanding of sediment transfers in river networks is key to our ability to characterize fluvial forms and their formative processes, to interpret historical channel trajectories, and predict future patterns (Fryirs, 2013). The combination of processes regulating sediment production, routing, and deposition across space and time is commonly referred to as sediment connectivity (Bracken et al., 2015; Wohl et al., 2018). Local sediment connectivity is the result of basin-scale processes that potentially connect an individual reach to the entire upstream river network. Thus, studying sediment connectivity requires a network scale consideration of the provenance, timing and quantity of sediment moving through the entire network, and how the sediment cascades originating from different sources interact with each other (Schmitt et al., 2017).

The theoretical definition of sediment connectivity has developed in parallel with the understanding of fluvial processes to represent the continuity of sediment transfer from a source to a sink (Downs et al., 2018). The concept of fluvial sediment connectivity is thus a powerful tool to link network scale processes to local morphology and to morpho-dynamics under natural and disturbed conditions. Over the last decade, emerging remote sensing technologies have fostered the generation of network-scale geomorphic datasets concerning, e.g., hydrology (Van Der Knijff et al., 2010) and channel morphology (Bizzi et al., 2019), and functional characteristics such as channel confinement and width of the active channel (Demarchi et al., 2017; Fryirs et al., 2019; Roux et al., 2015). Given this newly available information, several modelling frameworks have been developed with the aim to simulate sediment transfer and quantify fluxes and, in some cases, provenances in channel networks (Czuba & Foufoula-Georgiou, 2014; Heckmann & Schwanghart, 2013; Schmitt et al., 2016). These pioneering experiences are of paramount importance to advance our capacity to infer basin scale sediment transfers and, ultimately, be able to predict foreseeable river behaviors, changes in channel characters and provide sediment management measures for the future (Schmitt et al., 2018; Schmitt et al., 2019).

However, our ability to validate results and judge the veracity of simulated network fluxes has been limited because data on sediment transport at network scale are often scarce or non-existent. Recent findings (Schmitt et al., 2017) proved that even few reaches with data on transported grainsizes and fluxes can significantly constrain the scenarios of basin-scale sediment connectivity patterns. Additionally, observable channel morphology could improve our ability to corroborate linkages between outputs of connectivity models and river processes. Since Schumm's river classification scheme (1985), and even earlier (Leopold and Wolman, 1957), our conceptual understanding of how sediment size and flux can affect channel morphology and planform is pretty clear. However, while this is true from a qualitatively point of view these links are far from being established in a quantitative manner.

Interestingly, amongst the various studies of network-scale sediment connectivity (Czuba, 2018; Gilbert & Wilcox, 2020; Schmitt et al., 2016), none have investigated links between network sediment connectivity and reach-scale transitions in channel patterns. This is a current limitation and an opportunity for the future since our ability to identify tipping points, i.e., sediment connectivity conditions, which can transform radically channel patterns, depends on that. For instance, empirical evidence highlights that braided rivers across the globe shifted towards sinuous single channels due to sediment starvation affecting channel stability, flood protection, and aquatic and riparian habitat quality over the last fifty-one hundred years (Bizzi et al., 2019; Kondolf, 1997; Liébault & Piegay, 2001; Piégay et al., 2009; Surian & Rinaldi, 2003). With those braided reaches, also unique fluvial habitats and ecosystem services were lost. For these reasons, establishing a quantitative link between modelled sediment connectivity (e.g., flux and size) and observed river morphology would thus advance our ability to: i) validate the meaning and validity of simulated network-scale sediment transport values, and ii) to predict future changes in channel morphology and morpho-dynamic behaviors under various conditions of sediment connectivity.

Discriminating a braided pattern from a single channel pattern has been of interest from the fundamental work of Leopold and Wolman (1957), who proposed a simple slope discharge discriminant relation, based on the hypothesis that for a given discharge, braided rivers are steeper. Since then, many authors tackled a similar research questions, proving that not only slope determines channel patterns but also bed particle size and stream power (van den Berg, 1995), width to depth ratios (Crosato and Mosselman, 2009; Fredsøe, 1978), and sediment concentration (Mueller and Pitlick, 2014). These authors proposed formulae to discriminate braided/non braided reaches, which have been applied always using field collected data. However, theoretically it is possible to feed them with outputs derived by network-scale sediment connectivity models providing information on, for instance, sediment concentration and grain size. Testing their performance would support model validation and, at the same time, allow to test these thresholds on much wider river reach samples, covering entire networks.

In this work, we implement the network-scale sediment connectivity model CASCADE (Schmitt et al., 2016; Tangi et al., 2019) for the Vjosa basin, which is considered one of the last wild rivers in Europe, due to the lack of major dams or barriers for the majority of its course and on most of its tributaries. The river Vjosa is a gravel-bed river showing various transitions from braided to single sinuous channel patterns across its course. The Vjosa also features some of the largest braided reaches still existing in Europe, which, as many Balkan rivers, are recognized as hotspot of biodiversity, while being threatened by numerous dam projects (Peters et al., 2021; Schiemer et al., 2018). The objective of this paper is to implement CASCADE in a data-scarce environment, testing an optimization routine to define grain size availability across the network, implementing a sensitivity analysis to explore the main source of uncertainties in sediment fluxes calculations, and use few selected field evidences to validate the model.

Once sediment fluxes and connectivity at the network scale are assessed and validated, we link them to channel patterns observed across the network. To do so, we test an empirical model proposed in literature to discern between Multi-Channels (MC) and Single Channel (SC) types based on sediment concentration, discharge and grain size (Mueller and Pitlick, 2014). The empirical model is fed by CASCADE outputs in terms of sediment concentration and D50, whereas channel patterns are observed by available orthophotos. Finally, we also use the findings to assess sensitivity of the Vjosa braided pattern to be lost if e.g., upstream hydropower dams would reduce sediment supply.

By this case study, the paper will discuss approaches to the initialization and validation of network-scale sediment connectivity models of general validity proving the significance of even few but strategically selected field evidence for validation. In so doing, the paper points out the opportunity of network scale modelling to leverage available scattered sediment data to a wider and more consistent understanding of network scale processes. This work will also prove the strength of the link between simulated sediment fluxes and observed channel patterns opening to the possibility to predict channel planform sensitivity to alternative scenarios of sediment management strategies at the basin scale, which is a critical issue for such a study case.

CASE STUDY

The Vjosa river is one of the last remaining free-flowing fluvial systems in Europe. The river originates in Greece, but most of its unimpeded 260 km course is in Albania. Almost all tributaries of the Vjosa are not regulated by any human infrastructures making the Vjosa stand out from other heavily modified Mediterranean rivers (Belletti et al., 2020).

In Greece, the river, locally named Aaos, passes thought the Vikos-Aaos National park, where it forms impressive canyons. After entering in Albania, the Vjosa is joined by the Sarantaporos river, which displays wide braided channel patterns upstream of its confluence with the Vjosa (see Figure 1). The Vjosa then flows in a narrow valley, maintaining a relatively small width, incised in low terraces made of conglomerates deposits. After passing through the Dragot gorge, the river meets one of its two main tributaries, the Drinos. The valley then widens, the slope reduces and the river forms impressive braided sections up to two kilometers wide. The second largest tributary, the Shushica, enters the Vjosa near its delta. In total, the river drains an area of 6,700 km^2 and discharges in average 204 m^3/s at its mouth.

The Vjosa falls into the pluvio-nival hydrological regime, with heavy rainfalls and consequent peak-flows in spring. While the average annual rainfall is around 1500 mm, in the upper, mountainous regions of the basin, where the coastal Mediterranean climate gives way to the continental climate, annual precipitations reach around 2500 mm/year (Schiemer et al., 2018).

Geologically, the Vjosa river crosses the active graben system and the active frontal thrust system of the Albanides. The Vjosa river drains through ophiolites, flysch deposits, carbonate rocks, and Quaternary sediments. Limestone and sandstone represent the majority of riverbed sediment. The Vjosa river has various levels of alluvial terraces and recent analyses show that their formation is mainly controlled by climate changes which occurred during the Pleistocene (Carcaillet et al., 2009). In the middle part, the river flows over flysch deposits and the existing gorges follow an E-W transverse (E–W) along the frontal active trust, and then meanders on the coastal plain to the Adriatic Sea in the west.

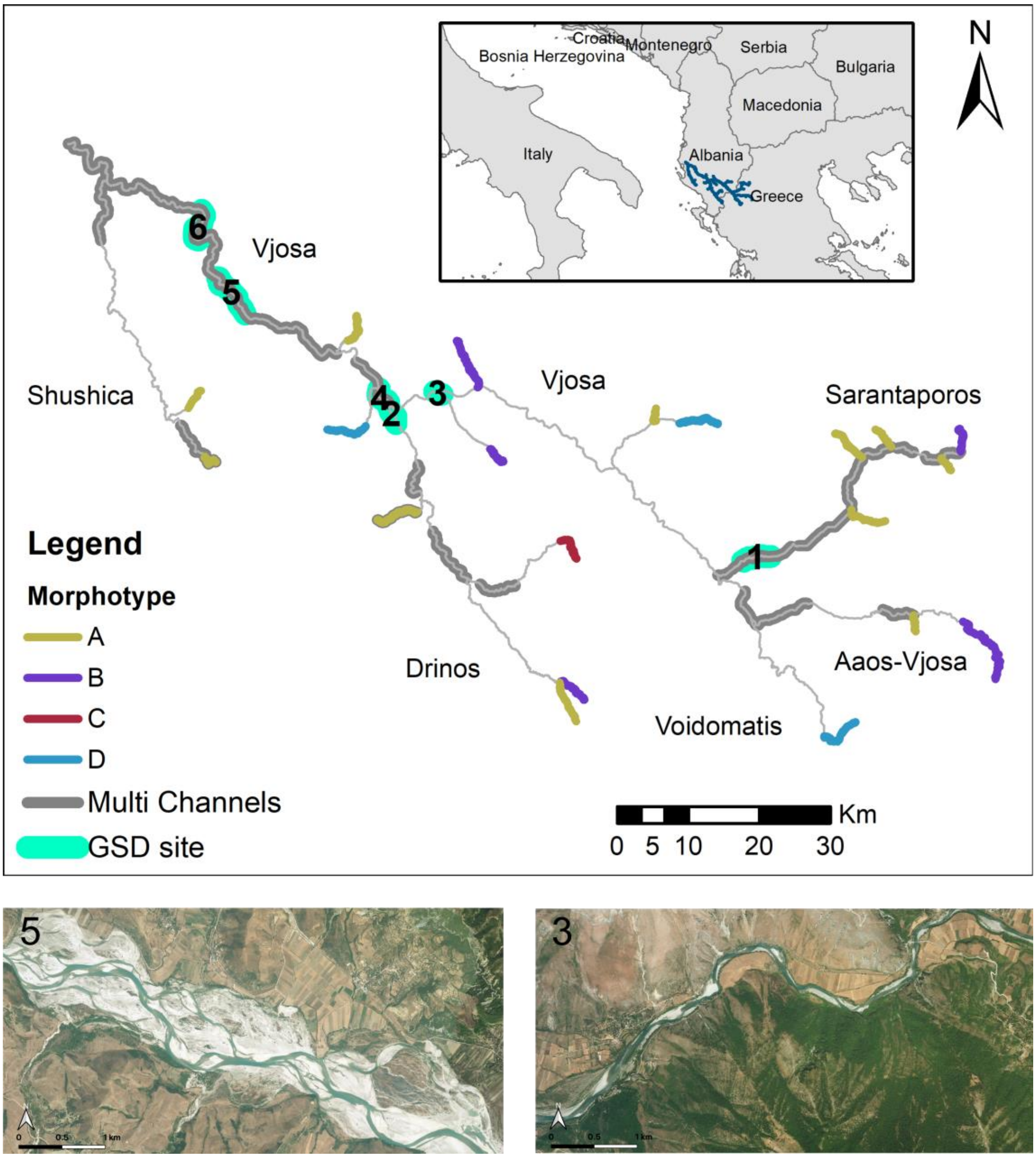

Figure 1- Location of the Vjosa river, the grain size distribution (GSD) sites for samplings, and the network representation of the river used in this paper. Note that the model domain

does not include the delta, to avoid DEM extraction errors in flat coastal areas. Multi channels are highlighted with a grey bold line. Morphotype are reported for source reaches (see Figure 3 for their definition). Two images around GSD sites 5 and 3 show two typical examples of Vjosa channel patters, a braided section upstream of Kalivaç (5) and a confined single channel patter east of the Dragot gorge (3) (both from Google Maps satellite images).

Due to this geological context, channel types, as described, display a remarkable variety: the river forms gorges and incises the terraces in the upper and middle catchment, and braiding channel patterns are then observed when the valley widens with a transition to meandering towards the mouth. We assume that the transition between braiding and single channel patterns is regulated by the magnitude and grainsize of sediment supply, the stream power, and the degree of confinement. Using CASCADE outputs, we aim to establish quantitative links between those single versus multi-channel pattern.

METHODS

The CASCADE model

The CASCADE model (CAtchment Sediment Connectivity And Delivery) (Schmitt et al., 2016) is a network-scale sediment transport model, which implements empirical sediment transport equations within a directed graph representing the river network (Tangi et al., 2019). CASCADE produces disaggregated information on sediment transport, deposition and delivery, allowing to track both the fate of sediment from a specific sediment source and the composition and origins of sediment in any downstream river reach. CASCADE has been applied in previous case studies to assess sediment connectivity in large river networks (Schmitt et al., 2016, 2017) and to evaluate alterations of sediment transport regime caused by anthropogenic alterations such as dams (Schmitt et al., 2018, 2019).

In the present study, we use the CASCADE toolbox (Tangi et al., 2019) to quantify bed load sediment fluxes in the Vjosa river network (Figure 1). CASCADE is a flexible and scalable tool to model network sediment connectivity using a relatively small number of remotely sensed and hydrological data to be calibrated. These include specification of the discharge, channel geometry and grain size distributions (GSDs) for each river reach (Figure 2). However, for the Vjosa, similar to probably most larger river systems worldwide, there are relatively few point measurements of GSDs. Here, we use an optimization routine, which was previously developed by Ferguson et al. (2015) for a single river channel. We expand the approach to an entire-network scale and use it to define bed

GSDs in all river reaches. In the next sections, we describe how transport capacity is calculated in CASCADE and how we implement the optimization routine. Then, we describe how we derive the reach attributes needed to calculate transport rates at the network scale.

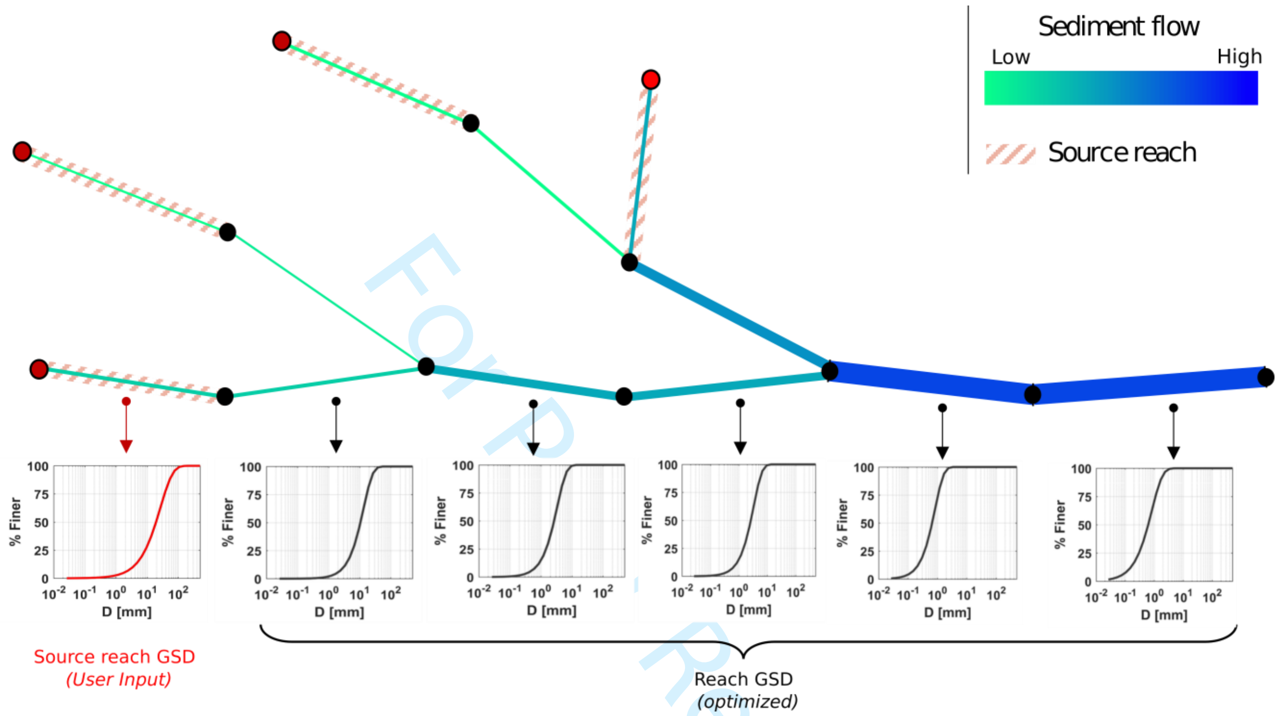

Figure 2 - CASCADE model conceptualization, for each reach the GSD are shown, source's reaches are highlighted in red.

Transport capacity calculation

The bed load transport capacity is calculated using a function presented by Parker & Klingeman (1982). This function is used primarily because it is formulated for sediment mixtures, and thus can predict transport rates of individual size fractions; this is important when trying to predict the GSDs from one reach to another. The subsurface- and surface-based versions of this function fit field data very well when calibrated to a reference shear stress (Parker & Klingeman, 1982; Mueller & Pitlick, 2014).

The bed load transport capacity for sediment size class *i* (Q_i^{sed} , [kg s^{-1}]) is defined as:

$$Q_i^{sed} = B_{at}\, W_i^*\, F_i\, \rho_s \left(\frac{\tau}{\rho}\right)^{3/2} (\Delta g)^{-1} \qquad \text{eqn.1}$$

where B_{at} is the channel width [m] over which active transport (at) occurs, W^*_i is the dimensionless transport rate for sediment size class *i*, F_i is the fraction of size class *i* in the bed surface sediment, ρ_s and ρ are the sediment and water density, respectively, g is the gravitational acceleration, and Δ is the submerged specific gravity of sediment.,

$$W_i^* = 11.2\left(1 - 0.853\,\frac{\tau_{r_i}}{\tau}\right)^{4.5} \qquad \text{eqn.2}$$

where τ is the bed shear stress [kg m^{-1} s^{-2}]:

$$\tau = \rho\, g\, H\, S \qquad \text{eqn.3}$$

and τ_{r_i} is the reference shear stress [kg m^{-1} s^{-2}] for an individual grain size, d_i [m]; τ_{r_i} is estimated from a hiding function:

$$\tau_{r_i} = \tau_{r_{50}} \left(\frac{D_i}{D_{50}}\right)^{\gamma} \qquad \text{eqn.4}$$

where $\tau_{r_{50}}$ is the reference shear stress [kg m^{-1} s^{-2}] for the median grain size, D_{50} [m] of the bed surface sediment; $\tau_{r_{50}}$ is estimated using an empirical equation presented by Mueller et al. (2005) that accounts for variations in the reference shear stress with increasing channel slope:

$$\tau_{r_{50}} = \rho\, g\, \Delta\, D_{50}\,(0.021 + 2.18\, S) \qquad \text{eqn.5}$$

The other variables in (3)-(5) are the mean depth, H [m], the reach-average slope, S [-], and the hiding function exponent, γ. Values of γ close to zero are indicative of conditions, where transport is weakly size-selective (equal mobility), whereas values of $\gamma > 0.1$ are indicative of conditions where transport is predominantly size-selective. The average flow depth is found using the Manning-Strickler formula (Manning et al, 1890). The fraction of each size class in the bed surface sediment layer F_i is extracted from the reach GSD. The total transport capacity of the reach is found by summing the transport capacity across all size classes.

<u>Initialization of GSDs for source reaches and routine for optimizing GSDs across the network</u>

Each first-order reach in the network is considered a source reach (these reaches are highlighted in red in Figure 2). To assign a grain size distribution (GSD) to each source, we visually classified the associated first-order reaches into four morphotypes as shown in Figure 3. Each morphotype was assigned a range of GSDs at the sources, based on Liébault's (2003) categorization and raw data of gravel GSDs in Mediterranean limestone mountain rivers.

Morphotype A (D50 from 27 mm to 48mm) is characterized by a large active channel width (defined here as the flow channels and unvegetated exposed gravel bar width) and narrow, well-defined low flow channels (possibly multiple channels); Morphotype B (D50 from 33 mm to 52 mm) is characterized by a single narrow low flow channel dominated by gravel (no boulders present) but with a narrower active width compared to Morphotype A; Morphotype C (D50 from 44mm to 79mm) has an active channel width of less than about 20m, with bed material consisting of gravel mixed with boulders. Morphotype D (D50 from 63mm to 100mm) is characterized by high density of boulders in the channel bed. Source morphotypes for the Vjosa network are indicated in Figure 1.

The GSDs for each of the remaining reaches are generated using the optimization routine proposed by Ferguson et al. (2015), where the GSD is adjusted until the sediment transport capacity within a reach is in equilibrium with the upstream sediment supply. The sediment supply of the source reaches is derived as follows. First, we assign source GSDs according to the above classification. Then, we calculate the transport capacity for the GSD based on local GSDs and hydromorphology. We finally assume that source reaches are in equilibrium too, i.e., sediment supply is equal to the local transport capacity.

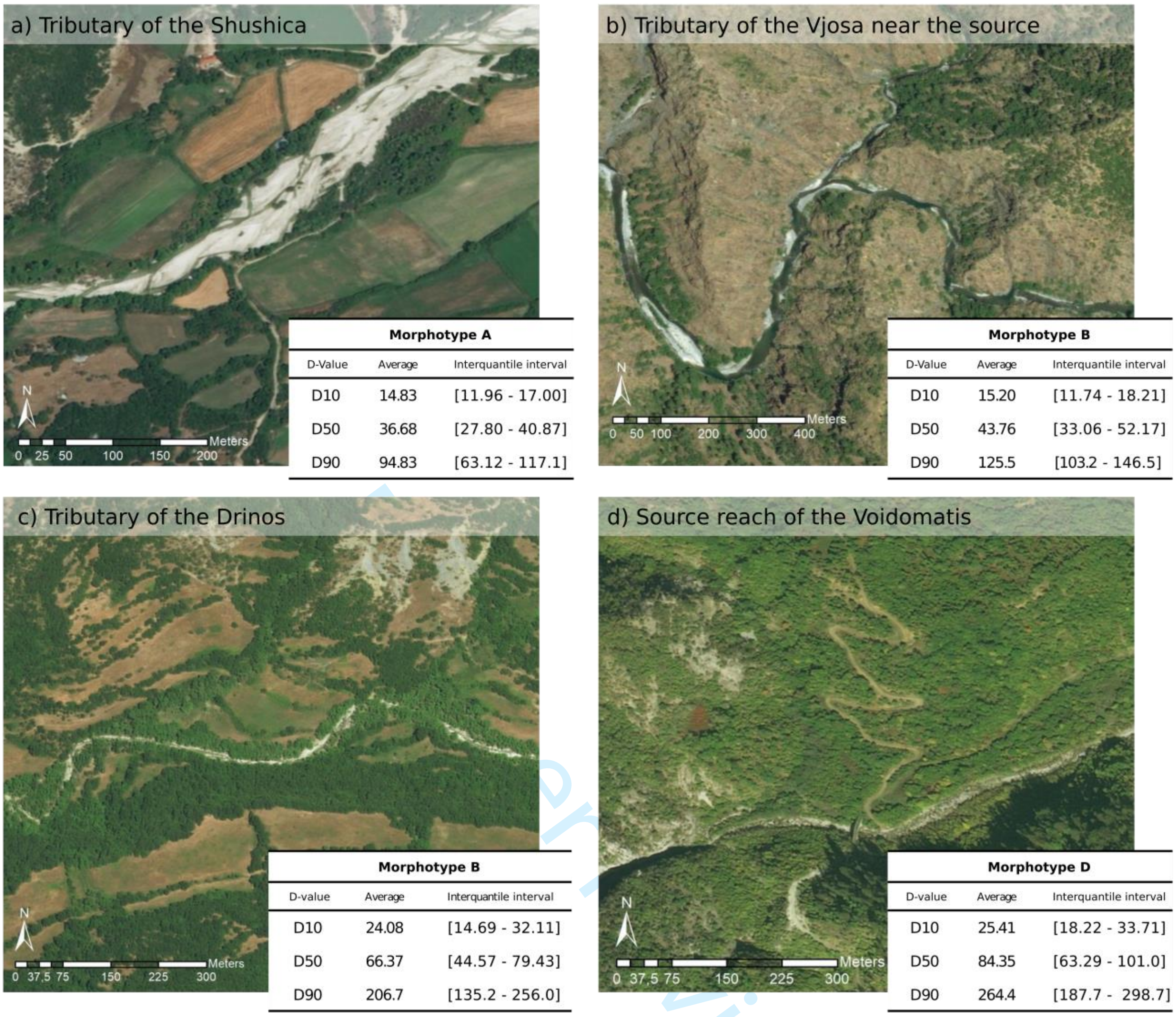

Morphotype A		
D-Value	Average	Interquantile interval
D10	14.83	[11.96 - 17.00]
D50	36.68	[27.80 - 40.87]
D90	94.83	[63.12 - 117.1]

Morphotype B		
D-Value	Average	Interquantile interval
D10	15.20	[11.74 - 18.21]
D50	43.76	[33.06 - 52.17]
D90	125.5	[103.2 - 146.5]

Morphotype B		
D-value	Average	Interquantile interval
D10	24.08	[14.69 - 32.11]
D50	66.37	[44.57 - 79.43]
D90	206.7	[135.2 - 256.0]

Morphotype D		
D-value	Average	Interquantile interval
D10	25.41	[18.22 - 33.71]
D50	84.35	[63.29 - 101.0]
D90	264.4	[187.7 - 298.7]

Figure 3 – Examples for four morphotypes used for classification of the source reaches (images from Google Earth). Morphotype A: wide active channel composed of alluvial gravel bars, with a low-flow channel relatively narrow in relation to the river bed; possible multiple channels. Morphotype B: active channel narrower than A, single and narrow low flow channel, sediment bars composed mostly by gravel, absence of emerging boulders; Morphotype C: Active channel usually less than 20m, presence of boulders. Morphotype D: Narrow active channel with high density of boulders in the bed.

For the remaining downstream reaches, the GSD is then determined by modifying the parameters of the Rosin distribution (Ferguson et al., 2015) a cumulative distribution function used to represent the range in bed material grain size (Shih and Komar, 1990)

$$F(< D) = 1 - \exp[(D/k)^{s}] \text{ eqn.6}$$

where k is the mode of the distribution and s an inverse measure of the spread. We then use the Genetic Algorithm toolbox in Matlab to minimize the difference between the local transport capacity in a reach and the incoming sediment flux from the upstream network by altering the two parameters s and k of the Rosin distribution. Each set of s and k results in a different set of frequencies, F_i (see eqn. 1), for each grain size class to be used in calculating the local bed load transport capacity.

Thus, we assume that the local GSD in a reach will change to accommodate sediment supply from upstream under local hydromorphologic conditions (gradient, width, discharge). Thus, network sediment flux only increases at confluences. However, changing the GSD implies that there can be erosion or deposition of specific size classes, resulting in specific morphodynamics. For example, if the optimization for a reach results in a GSD that is finer than the incoming GSD this fining could be related to either fine material being eroded from the channel or to deposition of coarse material. In each reach, to maintain equilibrium, the deposition of some sizes is compensated by the entrainment of others. This process generates GSD patterns across the network.

Defining river network reaches

In this section, we define how the river network was extracted from the available Digital elevation Model (DEM), and how it was segmented into river reaches with specific channel attributes, such as slope and channel type. For the Vjosa, we extracted the river network using the TanDEM-X DEM (Rizzoli et al., 2017; Wessel, 2018), with a pixel spacing of 0.4 arcsec, corresponding to a ground accuracy of approximately 10.9 m across the study area, and absolute vertical accuracy of less than 10 m. The network was defined using a combination of the CASCADE toolbox (Tangi et al., 2019) and Topotoolbox (Schwanghart and Kuhn, 2010). We set a minimum drainage area of 100 km^2 to identify the river network to be simulated. The river network is defined as a connected graph consisting of nodes linked to directed edges. Each edge represents a reach of the river network and is assigned a set of physical attributes including average slope, active channel width, channel roughness coefficient, bed material grain size distribution and discharge (Schmitt et al., 2016). These hydromorphic properties are then used to estimate the reach-scale sediment transport capacity, eqns. 1-5, from which we construct a reach-scale sediment budget, i.e., the balance between sediment supply and transport capacity, and the volume of sediment exported or deposited

Because each edge in the river network has a single set of attributes, the corresponding river reach should have quasi-uniform geomorphological features. We thus manually segmented the river network by visually identifying reaches with homogenous channel planform patterns, focusing particularly on differences in active channel width. Local channel widths were measured on available orthophotos from the most recent Google Earth images by selecting active sections of the riverbed with little or no vegetation. A total of 400 river width measures were extracted from orthophotos before proceeding to network segmentation. The resulting river network is divided into 139 reaches, with average length of 4.3 km. Reaches with multiple channel width measures were attributed an active width equal to the average of these measures.

Channel gradients were calculated from the DEM based on the elevation difference between the upstream and downstream node of each reach. Each reach was then classified as multi-channel or single thread, as shown in Figure 1. We also collected information on confinement, differentiating between confined or unconfined channels. Confinement was evaluated from orthophotos and reaches were classified as confined where terraces and hillslopes adjacent to the channels were visible. Channels bordered by floodplains were classified as unconfined.

River Network Hydrology

The magnitude and frequency of discharges used to calculate sediment loads for each river reach were estimated using a hydrological model. The dataset was generated by the LISFLOOD model, a rainfall-runoff model which provides daily flow data across a 5km x 5km grid (Forzieri et al., 2014; Van Der Knijff et al., 2010). Model simulations provided daily discharge data from 1990 to 2014. We assigned each reach in the CASCADE model to the grid cell of the hydrological model with which it had most overlap. From that cell, we then extracted the hydrologic time series and divided it into eight discharge classes corresponding to specific percentiles (0, 0.1, 2.3, 15.9 ,50, 84.1, 97.7, 99.9, 100). We also determined the frequency with which discharge was in each percentile. Thus, we assigned eight discharge classes and time fraction to each reach, which we then used to simulate daily sediment loads (in kg/s), which are aggregated using the annual frequency of each discharge to obtain the annual sediment flux.

<u>Relation between channel width and discharge</u>

Active transport widths along the Vjosa River can vary appreciably with water discharge, particularly in braided reaches. To account for these variations, we developed a rating curve between active transport width and discharge that could be applied to each reach. A rating curve such as this is needed because the calculations of bed load transport capacity are sensitive to variations in channel width and depth. There is no detailed information on channel cross sections from the Vjosa. Thus, we took an empirical approach, forming a relation between discharge and active transport channel width for each reach. Lugo et al. (2015) presented a relationship between dimensionless stream power (ω^*) and the ratio between active transport width and water width (Figure 4):

$$\omega^* = \frac{Q\ S}{B_w\sqrt{g\Delta\ D_{50}^3}} \qquad \text{eqn. 7}$$

where Q is the flow discharge, and B_w is the water width. The relationship calculated by interpolation of the data in Figure 4 is:

$$r = \frac{B_{at}}{B_w} = \max(0.2, min(2.36\ \ \omega^* + 0.09,1)) \qquad \text{eqn.8}$$

where *r* is the ratio between active transport width (B_{at}) and water width (B_w).

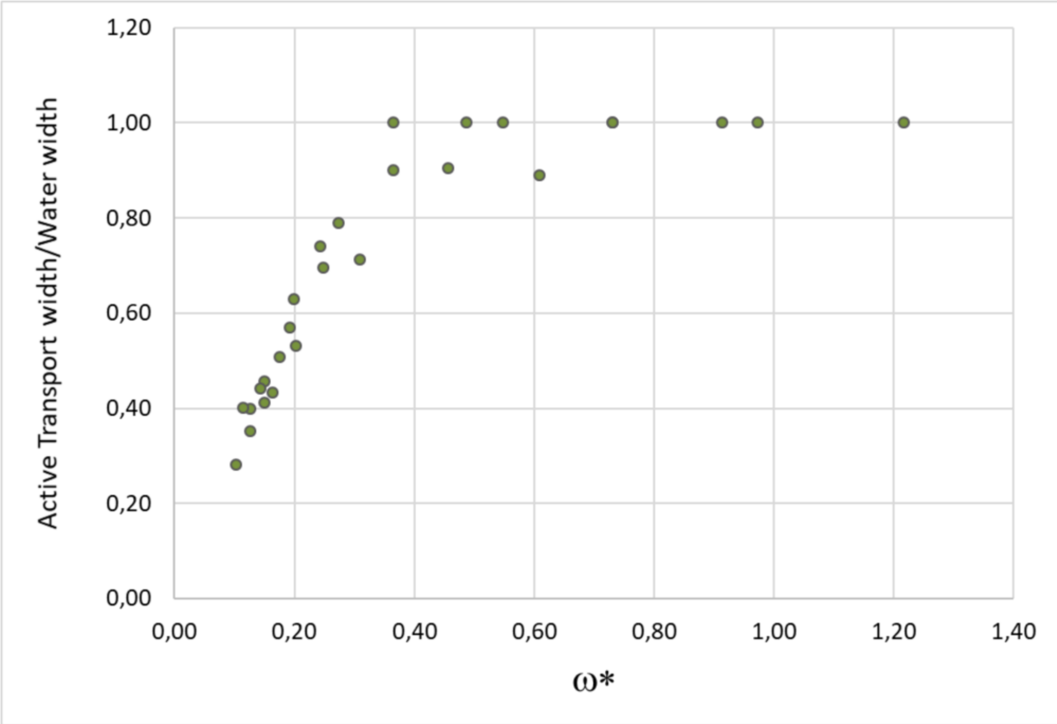

Figure 4 – The ratio of active transport width (B_{at}) with water width (B_w) plotted versus the dimensionless stream power (ω^*). Data from Lugo et al. (2015)

In the flume experiments conducted by Lugo et al. (2015), the active transport width corresponds to the portion of the channel where bed load sediment transport occurs, whereas the water width refers to the portion of the channel covered by water. For our purposes, we assumed that the values of active channel width measured along the Vjosa on Google Earth images (see previous section) correspond with the water width of their flume experiments. This is likely reasonable only for discharges with return period of two or more years, whereas could be overestimating it for discharges that are big enough to transport sediment but not necessary flooding the entire active channel. We are aware of the inherent uncertainty related to this estimate of active transport width and also of its importance in the implementation of the sediment transport model and for this reason it will be included in the sensitivity analysis discussed below. Dimensionless stream power is computed within CASCADE and then a value of the ratio (*r*) is derived for each reach and discharge scenario. The measured active channel width from orthophotos is then multiplied by this ratio (*r*) to obtain the active transport width (B_{at}) to be used to calculate transport capacity (see eqn.1).

Sensitivity Analysis

We implemented a global sensitivity analysis on key parameters used in the CASCADE simulations, focusing on source GSDs, the hiding function exponent γ, and the active transport width B_{at}. Source GSDs are not known and are provided in terms of plausible ranges for each morphotype (see tables of Figure 3). The hiding function exponent γ is allowed to vary from 0 to 0.1 to examine how differences in particle mobility affect downstream trends in GSDs. To consider the uncertainty in active transport width, B_{at} is randomly perturbed by a uniform distribution around plus or minus the 20% of the central estimates we derived using Lugo et al. (2015) method. We aim at assessing how these ranges of parameter uncertainties simultaneously affect the modeled sediment fluxes and GSDs. In this analysis we do not investigate the relative importance of each of these factors, which would require additional consideration of parameters covariance. Here, we only assess the uncertainty in sediment transport measures (total load and GSD in each reach) as a cumulative result of uncertainty in individual parameters. We use the Sobol' method, a technique to perform global sensitivity analysis (Hadka, 2015). For each parameter that is included in the sensitivity analysis (GSDs, hiding factors and active transport channel width) values are sampled between the proposed ranges to best cover the parameter space. For our case study, this resulted in 2300 independent parameter sets, with each set containing a distinct value for each of the three parameters. For each of parameter set, we performed eight CASCADE runs, one for each discharge percentile, to generate the estimates of GSD and annual bed load transport rates in each reach estimates. The analysis of 2300 CASCADE simulations allow us to assess uncertainty domains for the estimated yearly sediment fluxes and associated GSD patterns.

Field Data for validation

We carried out field surveys and collected grain size data in 6 reaches in February 2018. We sampled the bed material in two braided reaches close the mouth of the Vjosa river (Pocem and Kalivaç), a more upstream single thread reach (Drinos), a confined reach in the Dragot gorge (Vjosa Gorge), a braided tributary reach with high sediment supply (Sarantaporos), and a single thread reach in another tributary (Drinos), see Figure 1 for site locations.

We took between 5 and 10 pictures of the bed at different locations on exposed gravel bars. We took pictures by using a digital camera positioned vertically and about 1.5 m above the ground. We placed a scale bar in each frame to pinpoint the measurement scale. Picture resolution is 4032×3024 [px] resulting in an average pixel dimension of 0.5 [mm/px] for the selected 1.5 m distance from the ground. GSDs were calculated using Base Grain software (Detert and Weitbrecht, 2013), an object detection software tool for the analysis and extraction of granulometric information from images of non-cohesive gravel beds. Base Grain automatically separates grain areas (coarser than 8 mm) and interstices filled with finer sediment in the image using filtering techniques to identify the area of each gravel particle in the field of view. From there, the software extracts the grain size distribution of the coarser (>8mm) fractions of the surface sediment. The distribution is then completed with an estimation of the fraction of the finer, non-detectable particles, via Fuller curve estimation (Fehr, 1987). From the GSDs we can derive metrics such as D_{16}, D_{50} and D_{84}.

Test of the threshold between single-and multi-thread channels

As noted in the introduction, links between network sediment connectivity and reach-scale transitions in channel patterns have not yet been studied. Here, we propose to calculate a braided threshold using CASCADE outputs to discern single and multi-thread-channels. Mueller and Pitlick (2014) modified the approach developed by Millar (2005) and Eaton et al. (2010) to derive an equation that predicts the threshold between single- (SC) and multi-thread channels (MC) on the basis of a threshold in sediment concentration, and an assumption that braided channels will form at width to depth ratios greater than 50. The Mueller-Pitlick threshold is based on a regime relation (eqn. 12b) presented by Millar (2005):

$$\frac{B_{bf}}{H} = 425Q^{*0.12}C'^{-2.30}\mu'^{-2.9} \qquad \text{eqn.9}$$

where B_{bf} is the river width and H the flow depth at bankfull discharge. μ' is a dimensionless ratio of the relative erodibility of the bank versus the bed material. Q^* is the dimensionless discharge defined as

$$Q^* = \frac{Q_{bf}}{\sqrt{(s-1)gD_{50}}\,D_{50}^2} \quad \text{eqn.10}$$

$C' = -log_{10}C$, where C is bed load sediment concentration, defined as the ratio of bankfull volumetric bed load discharge, Q_{bf}^{sed} (m^3/s), to bankfull water discharge (m^3/s), Q_{bf} ($C = Q_{bv,bf}/Q_{bf}$) (Mueller and Pitlick, 2014). Equation 9 can be rearranged and simplified to find the critical sediment concentration, C_t, under the assumption of $B_{bf}/H=50$:

$$C_t = 10^{(-2.54Q^{*0.052}\mu'^{-1.26})} \quad \text{eqn.11}$$

Equation 11 defines the threshold between MC and SC patterns. We applied this formula to all alluvial unconfined or semiconfined reaches present within the Vjosa network. We neglected confined reaches because, in most cases, channels in these reaches are nonalluvial. Sediment concentration and grain size values for implementing equation 11 are derived by CASCADE simulations.

In order to further test the validity of CASCADE outputs, we also plot the braided threshold proposed by Eaton et al. (2010) depending on slope (S) and not on sediment concentration:

$$S_t = 0.4Q^{*-0.43}\mu'^{1.41} \quad \text{eqn. 12}$$

where S_t is the critical slope derived for the threshold case where $B_{bf}/H = 50$.

We then calibrated these thresholds (eqn. 11 and 12) altering the value of μ' to find the threshold that best discerns SC from MC patterns in the Vjosa basin, as also proposed by Millar (2005). The value of μ' so obtained incorporates all errors, including systematic errors in the theoretical relations. However, this approach is necessary to include how vegetation density and bank material affect the resistance to erosion. μ' near 1.0 is used for the most sparsely vegetated categories, indicating that bed and banks are approximately equally erodible, and progressively increase with vegetation density or changes in bank material towards more resistance texture to between 1.5 and 1.9 for the most densely vegetated channels.

Results

CASCADE validation

Figure 5 shows the pattern of mean D_{50} generated by CASCADE (the average value over 2300 simulations) for the entire network. In general, modelled grain size distributions are coarsest in headwater reaches and in single-thread reaches upstream of the Vjosa Gorge. An overall pattern of downstream fining is evident at the network scale. Figure 5 compares the GSDs generated by the 2300 CASCADE simulations for each reach (red lines) with the measured GSDs for the same reaches (green lines). In general, the CASCADE generated GSDs match the patterns observed in the field (Figure 5 and Table 1): the coarser grain sizes which are located along the Drinos and Sarantaporos tributaries and in the Vjosa Gorge are well-differentiated from the finer grain sizes in the downstream braided reaches, Vjosa-Drinos, Kalivac, and Pocem, respectively. The modeled GSDs broadly overlap with the measured GSDs, particularly in the four reaches above the Vjosa-Drinos confluence. In the two downstream reaches– Kalivac and Pocem– the modeled GSDs are generally finer than the measured GSDs, although the mean distributions (indicated by the bold solid lines) are quite close (Fig. 5). The percentile values listed in Table 1 suggest that the modeled D_{84} and D_{50} are comparable to Base Grain estimates across all sites. In contrast, it appears that the finer grain sizes simulated by CASCADE, e.g. D_{16}, are biased, overestimating their sizes in comparison to Base Grain estimates.

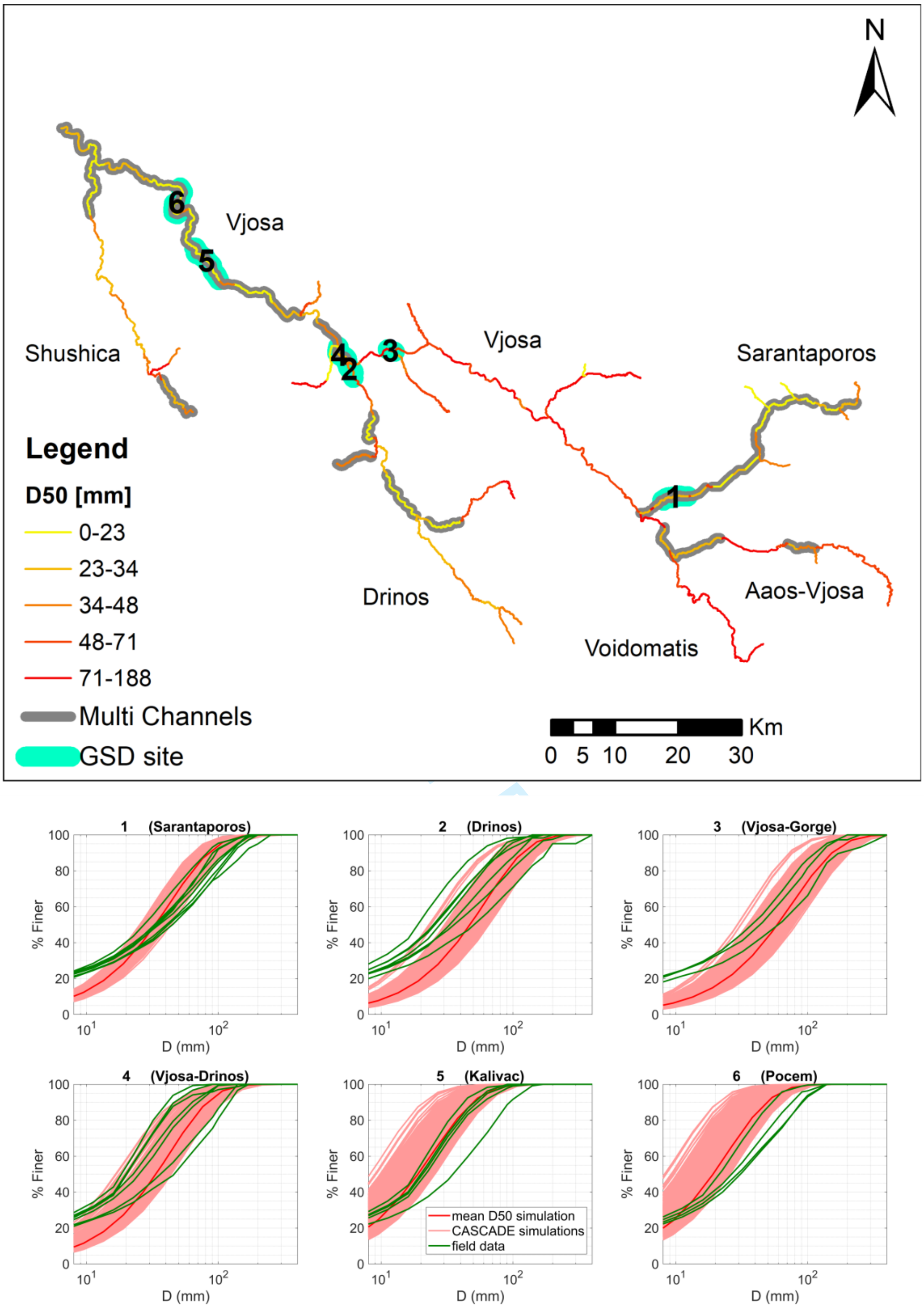

Figure 5 – At the top the river network shows range in mean D50, amongst all the 2300 simulations. GSD sampling locations are shown together with multi-channel patterns. At the bottom GSD sites show the grain size distributions modelled and observed (the numbers in the graph titles match the GSD site numbers in the top map). Green lines are GSD for each

picture derived by Base Grain, in red the CASCADE set of simulated GSDs, bold red line shows the mean among all the simulations.

	D_{16}	D_{50}	D_{84}	**Source**
Sarantaporos	11	33	72	Modelled
	4	36	97	Observed
Drinos	16	47	98	Modelled
	3	31	83	Observed
Vjosa-gorge	20	58	125	Modelled
	4	41	100	Observed
Vjosa-Drinos	11	33	70	Modelled
	3	27	61	Observed
Kalivac	6	19	40	Modelled
	2	20	42	Observed
Pocem	6	26	40	Modelled
	3	27	66	Observed

Table 1 – Modelled and observed D_{84}, D_{50} and D_{16} values for 6 reaches are reported in mm. Modelled values report the average amongst the 23000 CASCADE simulations (red bold lines in Figure 5-A). Observed values the average between the Base-Grain estimations from pictures (green lines in Figure 5-A). For site locations see Figure 5-B.

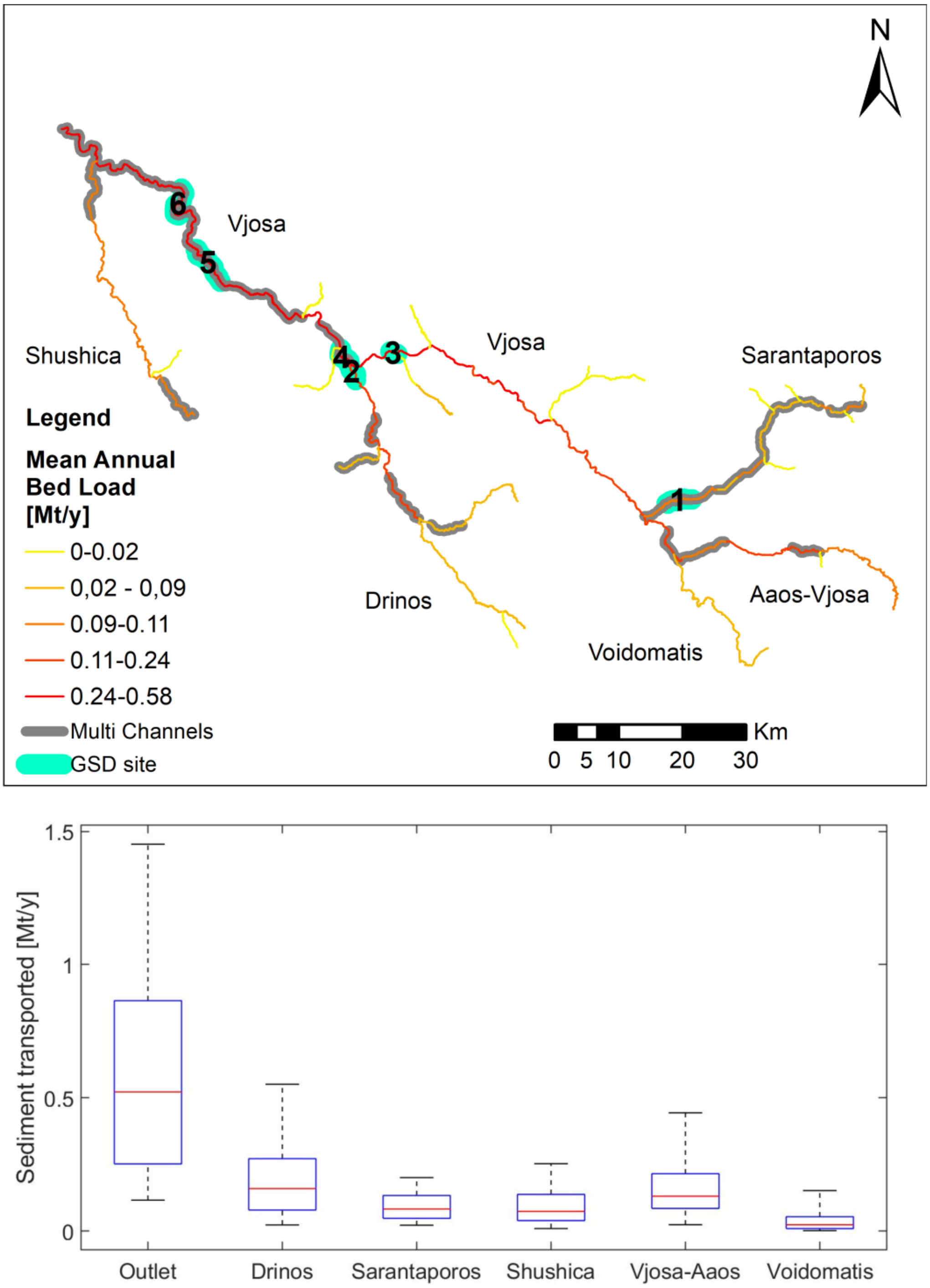

Figure 6 – Top figure: mean (across the 2300 simulations) yearly bed load transport values are reported across the network for all reaches, multi-thread channels (MC) reaches are represented by double lines in gray. Panel B: the boxplots report the range of yearly bed load values generated by CASCADE simulations at the outlets for the Vjosa and its main tributaries (the values correspond to the fluxes of the last reach of the tributary before the confluence with the Vjosa river). The red central mark in the boxplot indicates the median, and the bottom and top edges of the box indicate the 25th and 75th percentiles, respectively. The whiskers extend to the most extreme data points not considered outliers.

The simulated annual bed load fluxes for the entire network are presented in Figure 6, which shows average values amongst all the 2300 simulations. Figure 6 shows also a series of box plots indicating the range of simulated fluxes for selected locations, including the outlet of the Vjosa River and its main tributaries. Bed load estimates from our sensitivity analysis indicate that the median annual bed load at the outlet of the Vjosa is approximately 0.58 Mt/yr with 50% of the simulated fluxes falling between 0.25 and 0.86 Mt/y. The simulated sediment fluxes can be validated only at the outlet, where a few published estimates of the annual suspended sediment load are available. Milliman and Farnsworth (2011) report that the annual suspended sediment load of the Vjosa River is approximately 8.3 Mt/y; in a separate study, Fouache et al. (2001) report a slightly lower load of 6.7 Mt/y. The bed-load fraction in the Vjosa is reported in the range of 15-20% of the total load (Ciavola, 1999). If we assume a somewhat broader range, e.g., that bed load is 10-20% of the total load (bed load plus suspended load), then the annual bed load flux should fall in the range of 0.7-2.1 Mt/yr, depending on which values of suspended load we use, and what assumptions we make about the fraction of bed load to total load. The differences between bed load fluxes estimated from suspended sediment measurements and the fluxes generated by the CASCADE simulations (0.58 Mt/yr at the Outlet) are not large and suggest that the simulated fluxes are within an order of magnitude of the expected fluxes.

<u>Multi-channel / single channel threshold</u>

We further analyzed results for a possible correlation between modelled bedload transport and observed channel patterns. The channel pattern threshold given by eq. 11 (Mueller and Pitlick, 2014) indicates that the distinction between MC and SC reaches depends on various factors, including sediment concentration, C, relative bank strength, μ', and dimensionless discharge, Q* (which in turn depends on Q_{bf} and D_{50}). Using average values amongst the 2300 simulations of sediment fluxes and D_{50} generated by CASCADE, we can plot sediment concentration versus Q* for all the unconfined reaches, and compare with the threshold relation, eqn. (11). The results are shown in Figure 7. Rectangles correspond to SC reaches and circles correspond to MC reaches. Colors refer to specific sub-basins, and the diagonal lines indicate thresholds corresponding to three assumed values of μ': 1.0, 1.24 and 1.28. With few exceptions the SC reaches are well-discriminated from the MC reach for an assumed valued of μ' = 1.28. The value of 1.24 is an example of a different threshold which could apply to reaches in the Shushica basin (light orange points). In order to further explore the threshold between SC and MC patterns, Figure 8 plots the slope-dependent threshold given by eqn. 12. Using this threshold, SC reaches (squares) are relatively well-discriminated from MC reaches (circles). Figure 8 plots the same three thresholds shown in Figure 7 for μ' equal to 1.0, 1.24 and 1.28. Compared to the concentration-based threshold, the slope-based threshold has a wider zone of overlap. Indeed, SC and MC reaches coexist primarily in between μ' values of 1 and 1.28.

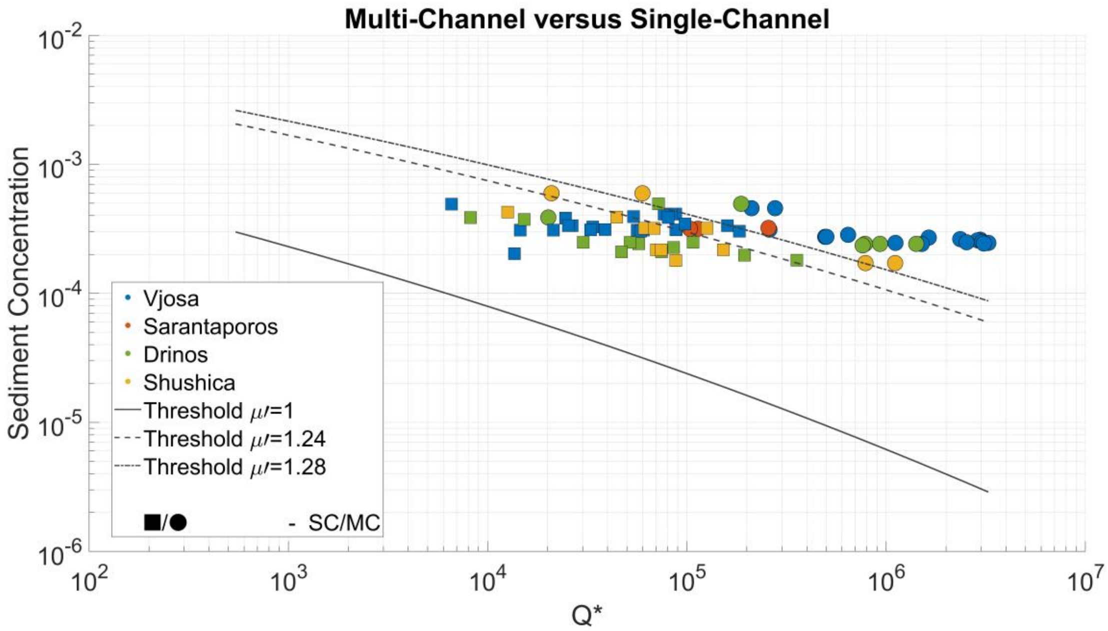

Figure 7 –Relation between sediment concentration and Q for all unconfined reaches. Circles represent multi-channel reaches (MC) and rectangles single channel reaches (SC). Colors refer to different sub-basins. Lines show alternative thresholds for braiding for different values of the relative bank strength parameter,* μ' = *1 (solid line), 1.24 (dashed line) and 1.28 (dash-dot line).*

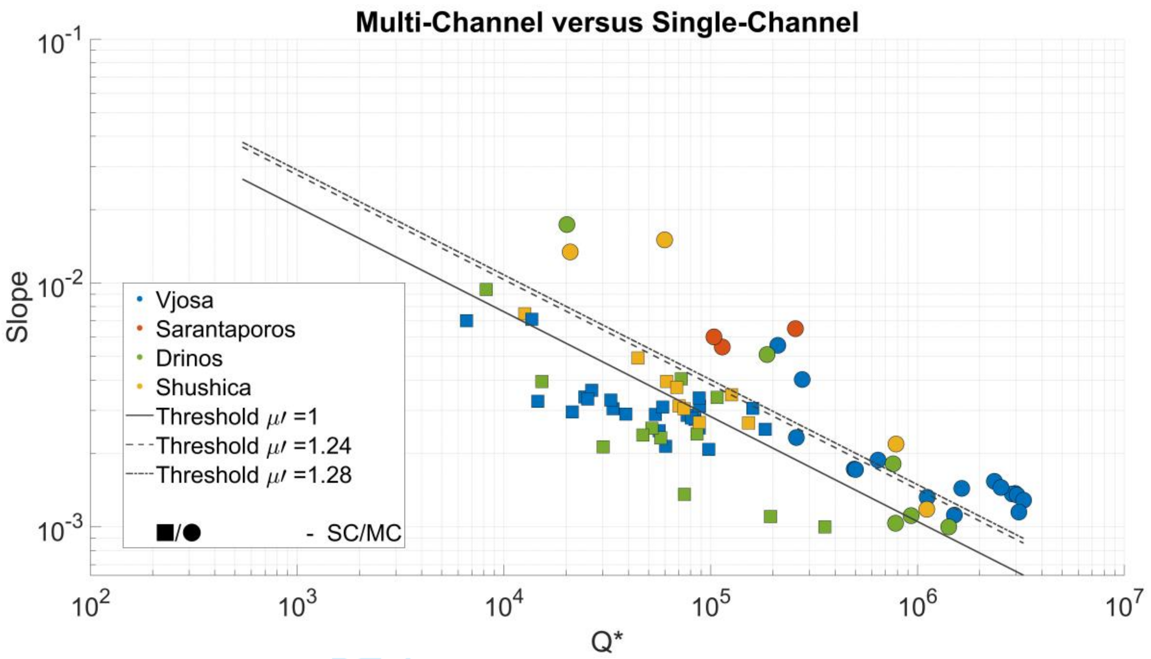

Figure 8 – Relation between slope and Q for all unconfined reaches. Circles represent multi-channel reaches (MC) and rectangles represent single channel reaches (SC). Lines show alternative thresholds for braiding for different values of the relative bank strength parameter μ’ = 1 (solid lines), 1.24 (dashed line) and 1.28 (dash-dot line).*

A third plot illustrating the combined influence of slope and grain size on channel pattern is shown in Figure 9. Here the symbol colors and sizes have the same meaning as in Figures 7 and 8, but D_{50} is plotted instead of Q* on the x axis, and dot sizes are proportional to active channel width normalized by drainage area. This latter parameter provides information on active channel width once the size effect of drainage area is removed (Bizzi et al., 2019; Piégay et al., 2009). The results shown in this figure indicate that, for similar values of channel slope, SC reaches are characterized by coarser D_{50} and lower values of normalized active channel width, whereas for similar values of D_{50}, MC reaches have higher slope and higher values of normalized active channel width. These observations suggest that the formation of MC patterns is likely driven by floodplain availability and degree of confinement. Indeed, when the channel can widen into the floodplain, it develops a MC pattern characterized by a wider active channel, which may in turn reduce the average depth, and thus lower the sediment transport capacity compared to SC reaches. The lower transport capacity may in turn trigger a condition for aggradation, as well as finer D50. In such cases, the MC reach needs a much higher slope than the SC reach to transport the same grain size.

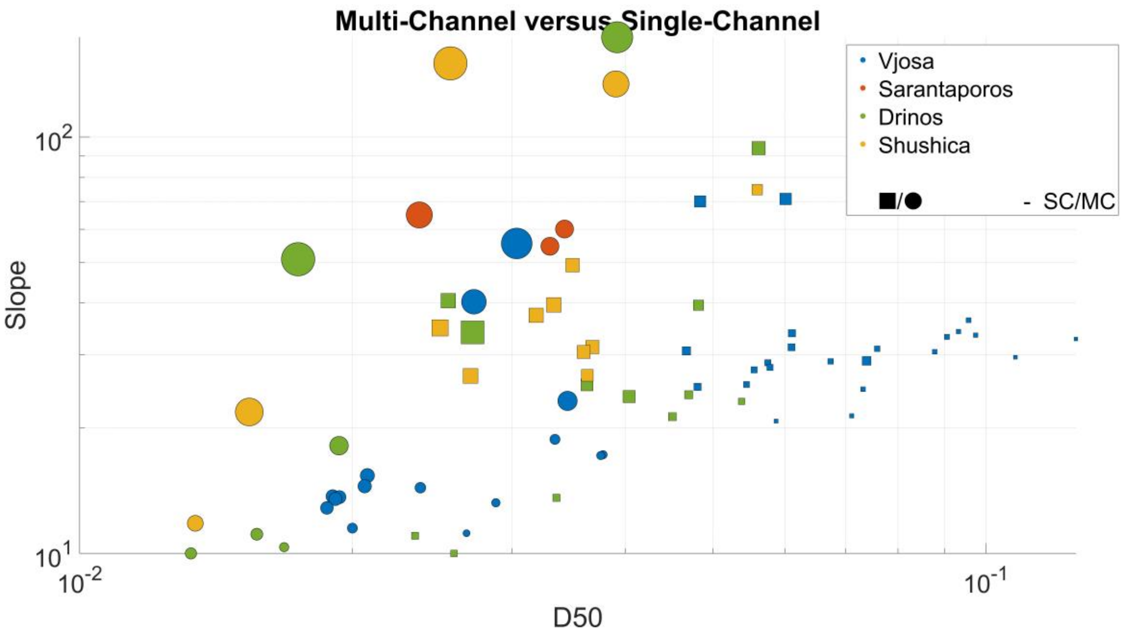

Figure 9 – Slope and D50 are plotted for all unconfined reaches: circles represent multi-channels (MC) and rectangle single channel (SC). Colors refer to different sub-basins, dot size is proportional to the active channel width normalized by drainage area. i.e., very large dots indicate reaches which are very wide relative to their drainage area.

It is evident from the results presented above that the discriminations between SC reaches and MC reaches are sensitive to the relative bank strength parameter, μ'. In addition, as explained in the Methods, we considered how uncertainties in other parameters (□, source GSDs and active width, B_{at}) might affect CASCADE outputs, and the discrimination between SC reaches and MC reaches. The results of our sensitivity analysis are summarized in Figure 10, which plots the 2300 simulated values of sediment concentration versus Q* for only the main stem reaches of the Vjosa River. The red rectangles are SC reaches and the blue circles show MC reaches. Filled markers indicate the mean values amongst the 2300 simulations for each type of reach. The line indicating the braided threshold corresponds to μ' = 1.28. The cloud of red and blue points indicating the CASCADE simulations shows that even when we include uncertainty in key parameters there is a clear separation between the two channel patterns along the Vjosa. An important trend that emerges, which was also evident in Figure 7, is that the range in simulated sediment concentration is relatively narrow. It appears, therefore, that concentration is less important compared to Q* in discerning SC from MC. This result is mostly driven by the modelling hypothesis that the sediment transport capacity within a reach is in equilibrium with the upstream sediment supply. This point is discussed further in the Discussion section.

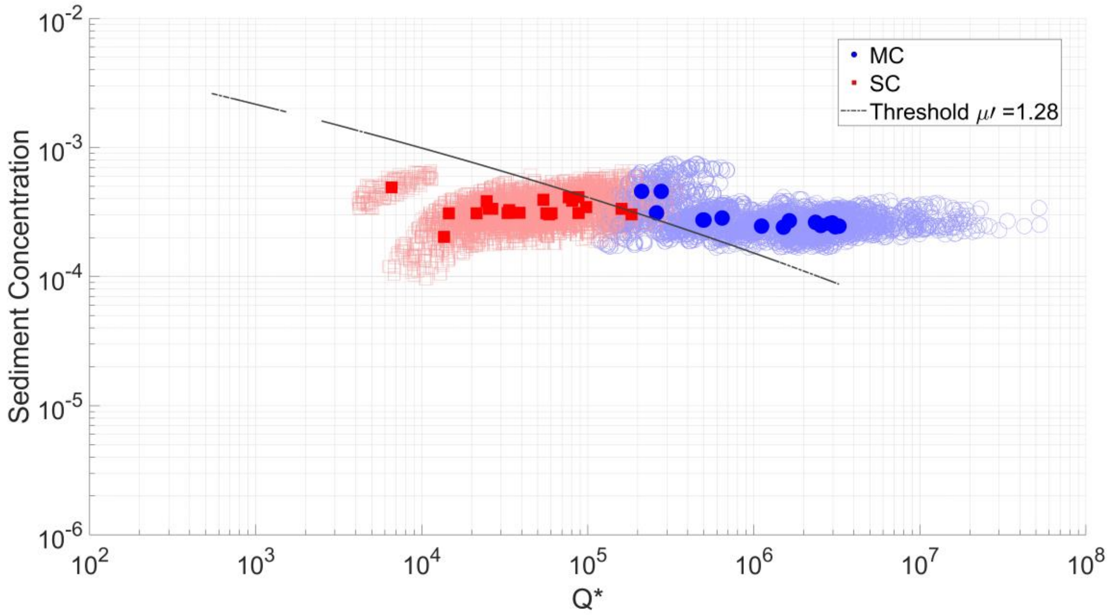

Figure 10 – Sediment Concentration and Q are plotted for all unconfined reaches along the main stem of the Vjosa. Red rectangles show single-channel (SC) reaches and blue circles multi-channels (MC) reaches. Filled markers indicate the mean value for each reach. The grey line indicates the braided threshold calculated with μ' equal to 1.28.*

Another practical result that emerges from this analysis is that once the SC-MC threshold is defined, river reaches close to the threshold are more likely shift from one pattern to the other compared to reaches further away from the threshold. Focusing on the Vjosa reaches and using average values amongst all the simulations, Figure 11 shows how reductions in sediment concentration could produce a channel-pattern shift with respect to the braided threshold. The MC reaches along the main stem of the Vjosa (circles in Figure 10 and 11) are all located downstream of the Drinos confluence (see Figure 6 or Figure 1) and Q* increases moving downstream. For the first six braided reaches downstream the Drinos confluence a sediment reduction of 40% would be sufficient to locate them near the braided threshold, whereas the most downstream ones would reach the threshold for a sediment reduction around 50-60%. This suggests that a sediment reduction of about half of the yearly sediment load would likely threaten the existence of the entire Vjosa braided system.

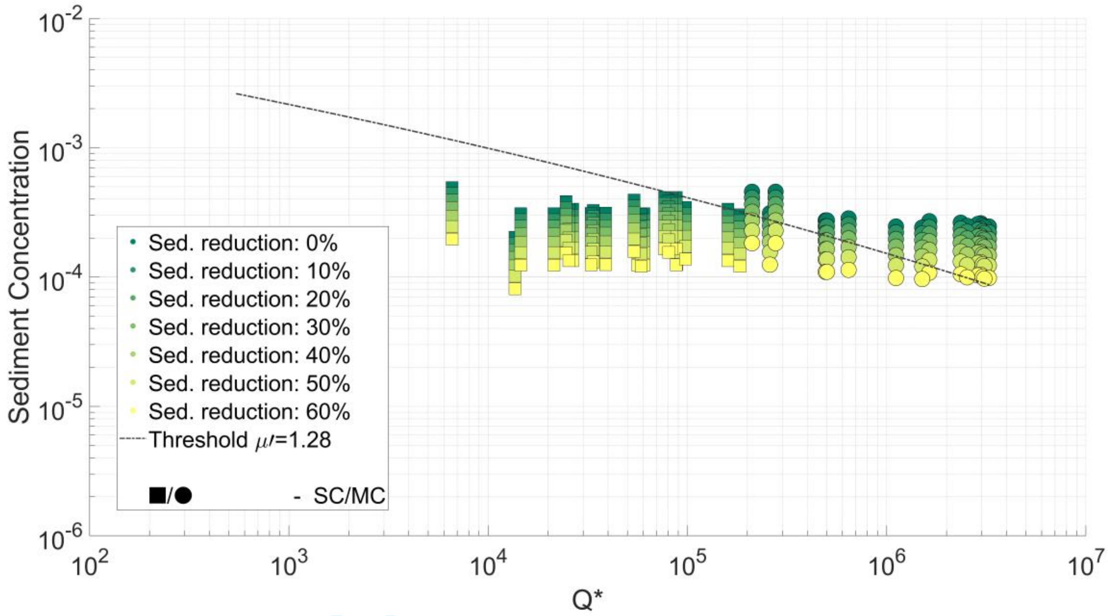

Figure 11 – Sediment Concentration and Q are plotted for all unconfined reaches along the main stem of the Vjosa: rectangles show single-channel (SC) and circles multi-channels (MC) reaches. Point color is proportional to the sediment reduction applied to each reach. The braided threshold (grey line) has μ' equal to 1.28.*

Discussion

<u>Model initialization and validation with GSD and sediment fluxes</u>

With this paper we aim to assess sediment connectivity in one of the last unimpaired braided rivers in Europe and to propose a method to robustly initialize and validate a network scale sediment connectivity model in a data scarce environment. The proposed approach demonstrates the importance of a few specific steps in model initialization which affect our system functioning hypotheses. First, we developed a hypothesis about the range of possible GSDs and sediment supply in source reaches (see Figure 3). We then assumed that subsequent reaches are in a morphodynamic equilibrium, i.e., that the transport capacity of the reach balances the upstream supply, similar to what Ferguson et al. (2015) proposed for the Fraser river. In addition, we performed a more in-depth sensitivity analysis. The significant degree of uncertainty in local sediment transport calculations is well known (Ancey, 2020a, 2020b) and this is even more critical in a data scarce environment. In the Vjosa, data on channel geometry is not available and hydrology is derived from a spatially distributed model with a coarse spatial resolution (Dankers & Feyen, 2009; Van Der Knijff et al., 2010). In addition to this reach-scale uncertainty, sediment transport in a reach depends on sediment supply from upstream, so these uncertainties and errors propagate and possibly amplify through the network. For this reason, we explored results based on a wide range of possible combination of source GSDs (see Figure 3) and different parameterizations of two sensitive variables in the sediment transport formula calculation: the hiding function exponent and the width-discharge relationship.

Despite the wide uncertainty in parameter values and scarce field data on grain size and sediment fluxes, the CASCADE simulations generate plausible and coherent patterns of sediment fining that match observed sediment size distributions along the Vjosa river and its tributaries (see Figure 5 and Table 1). The CASCADE-generated estimates of D_{50} and D_{84} are comparable to those observed in the field, whereas the model overestimates the size of the finer fractions. The bias in finer sizes is mostly a numerical effect related to the difficulty of resolving grain sizes finer than 8 mm with the Base Grain software. In the two most downstream reaches, Pocem and Kalivac, the modeled GSDs are overall finer than the measured GDS, but the mean distributions are similar. This effect for the downstream reaches is mostly due to two aspects of the modelling framework: i) CASCADE simulates transport across all sediment size classes defined in the network and finer sediment might be underestimated in our observed measures of surface grain sizes, e.g., because of armoring; (2) as mentioned before the fine part of the distribution tail cannot be easily compared. Volumetric sampling would be required in this situation, and that would likely produce finer distribution compared to surficial samples.

The hydrologic model adopted is validated at the European scale but without data from this basin (Van Der Knijff et al., 2010). For this reason, in the absence of better hydrological data is not possible to predict how this affects model results. With this in mind, we believe that our estimations of sediment fluxes in the Vjosa network are in the same order of magnitude as those reported in the literature (Covault et al., 2013; Fouache et al., 2001; Milliman and Farnsworth, 2011), and the approach illustrates how we can leverage available data to build a more consistent understanding of sediment connectivity.

Linking sediment fluxes and GSD with river morphology

In spite of limited data availability the Vjosa River basin provides a valuable opportunity to evaluate the link between modelled sediment fluxes and river morphology. The link between sediment connectivity and river channel type has been discussed in a number of papers (Buffington & Montgomery, 2013; Knighton, 1998; Kondolf et al., 2003; Schumm, 1985), but a quantification of these physical links is often missing. To this aim, we applied a threshold formula to discern MC from SC based either on sediment concentration as proposed by Millar (2005) and Mueller and Pitlick (2014), or slope, as proposed by Eaton et al. (2010). Such a threshold is particularly meaningful for the Vjosa basin since here the river network experiences various transitions throughout its course from a multi-thread to single-channel pattern. Although the classification between these river planform types has been based on expert judgment, we believe the ability to discern between MC, where more than a single low-flow channel is well developed, from purely SC ones, is robust.

Our findings support previous models developed to discriminate between multi- and single-thread channel patterns and highlight that the MC/SC transition can be robustly modelled even under uncertainty (Figure 10). Our results suggest that the transition between MC and SC patterns is well defined by a threshold that varies with sediment concentration and relative bank strength, μ'. We treated μ' as a calibration parameter but note that it incorporates all errors, including systematic errors in the theoretical relations. The importance of this parameter in discerning SC from MC patterns has been discussed in a recent review (Candel et al., 2020). Analyzing what differentiates MC from SC reaches (Figure 9), we have confirmed a clear pattern that can be interpreted as follows. The channel's ability to widen into the floodplain is a primary driver of the formation of MC reaches, which are characterized by a higher channel width, lower channel depth, finer grain sizes, and possibly higher slopes compared to adjacent SC reaches. This interpretation reinforces the idea that bank strength, floodplain availability, and sediment composition are critical parameters in the formation of braided reaches, as discussed in the work of Candel et al. (2020) and Hohensinner et al. (2021).

We have shown that CASCADE modelling outputs can be used to establish thresholds between multi- and single thread channels. To our knowledge, this is the first time that such thresholds are used in a dynamic context with simulated data and not field data. This is also the first time that the threshold theory has been applied to alluvial reaches in an entire river network. This has not been done in the past because the data needed to implement the underlying equations (Eaton et al., 2010; Millar, 2005) are generally not available continuously across the network. This is an important step towards quantifying the link between connectivity and fluvial forms at the basin scale and in assessing channel sensitivity to change.

The information emerging from Figure 7, 8 and 9 supports also a further comment about CASCADE simulations, which does not emerge looking only at GSD and fluxes at the outlet. Indeed, the Sarantoporos is a braided tributary of the Vjosa represented by red dots in Figure 7, 8 and 9. We can note that these reaches have slope, Q*, normalize active channel width and D_{50} to be clearly classified as MC reaches, whereas in Figure 7 they appear close or just below the braided threshold for μ' at 1.28 due to low values of sediment concentration. This incoherence suggests that simulated sediment fluxes for this basin are likely underestimated. This could be due to: i) underestimation of discharges due to the discussed limits of the adopted hydrological model, particularly likely for a large-scale model such as LISFLOOD when it provides estimates of small upstream basins, such as the Sarantoporos; ii) inadequacy of the sediment equilibrium hypothesis particularly likely in a very dynamic and sediment rich sub-basin, such as the Sarantoporos. This latter point has probably wider implications beyond the Sarantoporos reaches. We already observed that the range of sediment fluxes generated by CASCADE is likely narrower than in reality. This is visible in particular in Figure 10 and 11 observing the range of sediment concentration values compared to the range of Q*. This result is due to the equilibrium hypothesis that allow sediment fluxes only to increase at the inlet of new confluences. Linking modelled sediment fluxes and river morphology allow then to further validate modelling hypothesis and outputs beyond GSD and sediment load data availability.

<u>Assessing river morphology sensitivity and implications for management</u>

A planform shift from braided or wandering channel patterns to single-thread patterns is a well-known consequence of alterations in water or sediment supply. In sediment starved rivers the changes can trigger a chain of reaction from river-bed incision, bank and infrastructure destabilization, aquatic and riparian habitat degradation and groundwater table alterations (Bizzi et al., 2015; Bizzi et al., 2019; Kondolf, 1997; Surian & Rinaldi, 2003). For this reason, being able to predict river channel response to alteration in sediment delivery is of paramount importance to support river management activities. Recent studies focusing on river sensitivity to changes in water and sediment supplies (Fryirs, 2017; Reid & Brierley, 2015) have highlighted the importance of understanding these links to be able to predict future channel change and better support river management strategies.

In the present study, we used average values of CASCADE simulations to calibrate the braided threshold with μ' at 1.28, then determined how different degrees of sediment reduction would move MC reaches toward and perhaps across the threshold for SC reaches.

This perspective is relevant for the Vjosa where hydropower development might alter one of the last undammed braided rivers in Europe (Peters et al., 2021; Schiemer et al., 2018). We have shown that halving the annual sediment load could transform the Vjosa from a braided river system to single thread.

Further studies are needed to assess the degree of accuracy of such a threshold. At what point in the sediment concentration-Q* plane would a river that today is braided turn into a river that is single channel? This is untested at the moment. The distinction between MC reaches and SC reaches clearly emerge but the distinction is based on the validity of model estimates and on the spatial distribution of reaches. What would be needed is information on some reference reaches for which we can determine their trajectories over time. To build such historical trajectories we need data on sediment transport and D50 for the past, which do not exist. What is more achievable is to start monitoring these trajectories in the future by mapping changes in channel morphology with respect to new positions in the sediment concentration-Q* plane. Such knowledge could then be integrated into more comprehensive assessments of how alterations in sediment load and hydrology, translate to changes in channel form and function. Those assessments can then be used to inform management strategies such as mining regulations or the strategic siting or removal of dams.

Conclusion

This paper presents the application of the CASCADE model to the Vjosa river. We demonstrate how to initialize a network-scale sediment connectivity model in a context where data on hydrology and sediment information are scarce. In order to include how various source of uncertainties about key river attributes affect the calculation of transport capacity, we performed a global sensitivity analysis. The GSDs generated by the model generally match observed GSDs, except in the two downstream-most reaches where the finest modeled sizes are underrepresented. The modeled bed load sediment fluxes increase systematically downstream, and annual fluxes at the outlet of the Vjosa are well within an order of magnitude of fluxes derived from previous estimates of the annual suspended sediment load.

In addition to these results, we link simulated sediment fluxes and grain size across the network to observed river channel planform types. We used published braiding thresholds, which require information on water and sediment discharges, to discern MC from SC patterns. Feeding the empirical threshold model with CASCADE outputs we are able to discern these two patterns after calibrating the relative bank strength parameter. This is a remarkable result because it is an additional form of validation which supports the hypothesis that simulated sediment fluxes and their size distributions across the network are realistic and coherently linked to observed channel patterns. It is the first time that the adopted braided threshold is calculated with data generated by a sediment transport model and not with field data. It is also the first time that model output is applied and validated continuously at the scale of an entire river network. Inconsistency in these relationships also highlights some relevant limitations of the model, related to discharge estimation and the sediment equilibrium hypothesis adopted.

The findings presented herein advance our ability to link sediment connectivity to river planform patterns and the sensitivity of the patterns to sediment management. For example, a 50% reduction of sediment transport along the main stem of the Vjosa, e.g., because of the proliferation of hydroelectric dams (Peters et al., 2021), would likely alter the unique braided character of the river. Future applications can develop more informed strategies for sediment management and tools to assess the consequences of network-scale alterations in sediment connectivity and channel planform stability.

Acknowledgment

This research was partially supported by the EC Horizon 2020 Research and Innovation Programme, AMBER (Adaptive Management of Barriers in European Rivers) Project, grant agreement number 689682. The TanDEM-X DEM was provided under the Tandem project id DEM_HYDR1516. We are thankful to Dr Ad de Roo from the Joint Research Centre of the European Commission for providing us the LISFLOOD hydrological data. We would like to thank Prof. Guido Zolezzi (University of Trento), Prof. Walter Bertoldi (University of Trento), and Prof. Klodian Skrame (University of Tirana) for their help in the field.

References

Ancey C. 2020a. Bedload transport: a walk between randomness and determinism. Part 1. The state of the art. Journal of Hydraulic Research **58** : 1–17. DOI: 10.1080/00221686.2019.1702594

Ancey C. 2020b. Bedload transport: a walk between randomness and determinism. Part 2. Challenges and prospects. Journal of Hydraulic Research **58** : 18–33. DOI: 10.1080/00221686.2019.1702595

Belletti B et al. 2020. More than one million barriers fragment Europe's rivers. Nature **588** : 436–441. DOI: 10.1038/s41586-020-3005-2

van den Berg JH. 1995. Prediction of alluvial channel pattern of perennial rivers. Geomorphology **12** : 259–279. DOI: 10.1016/0169-555X(95)00014-V

Bizzi, S, Dinh Quang, Bernardi Dario, Denaro Simona, Schippa Leonardo, Soncini-Sessa Rodolfo. 2015. On the control of riverbed incision induced by run-of-river power plant. Water Resources Research **51** : 5023–5040. DOI: 10.1002/2014WR016237

Bizzi S, Piégay H, Demarchi L, Bund WV de, Weissteiner CJ, Gob F. 2019. LiDAR-based fluvial remote sensing to assess 50–100-year human-driven channel changes at a regional level: The case of the Piedmont Region, Italy. Earth Surface Processes and Landforms **44** : 471–489. DOI: 10.1002/esp.4509

Bracken LJ, Turnbull L, Wainwright J, Bogaart P. 2015. Sediment connectivity: a framework for understanding sediment transfer at multiple scales. Earth Surface Processes and Landforms **40** : 177–188. DOI: 10.1002/esp.3635

Buffington JM, Montgomery DR. 2013. Geomorphic classification of rivers. In: Shroder, J.; Wohl, E., ed. Treatise on Geomorphology; Fluvial Geomorphology, Vol. 9. San Diego, CA: Academic Press. p. 730-767. : 730–767.

Candel J, Kleinhans M, Makaske B, Wallinga J. 2020. Predicting river channel pattern based on stream power, bed material and bank strength. Progress in Physical Geography: Earth and Environment : 0309133320948831. DOI: 10.1177/0309133320948831

Carcaillet J, Mugnier JL, Koçi R, Jouanne F. 2009. Uplift and active tectonics of southern Albania inferred from incision of alluvial terraces. Quaternary Research **71** : 465–476. DOI: 10.1016/j.yqres.2009.01.002

Ciavola P. 1999. Relation between river dynamics and coastal changes in Albania: An assessment integrating satellite imagery with historical data. International Journal of Remote Sensing **20** : 561–584. DOI: 10.1080/014311699213343

Covault JA, Craddock WH, Romans BW, Fildani A, Gosai M. 2013. Spatial and Temporal Variations in Landscape Evolution: Historic and Longer-Term Sediment Flux through Global Catchments. The Journal of Geology **121** : 35–56. DOI: 10.1086/668680

Crosato A, Mosselman E. 2009. Simple physics-based predictor for the number of river bars and the transition between meandering and braiding. Water Resources Research **45** DOI: 10.1029/2008WR007242 [online] Available from: https://agupubs.onlinelibrary.wiley.com/doi/abs/10.1029/2008WR007242 (Accessed 17 January 2020)

Czuba JA. 2018. A Lagrangian framework for exploring complexities of mixed-size sediment transport in gravel-bedded river networks. Geomorphology **321** : 146–152. DOI: 10.1016/j.geomorph.2018.08.031

Czuba JA, Foufoula-Georgiou E. 2014. A network-based framework for identifying potential synchronizations and amplifications of sediment delivery in river basins. Water Resources Research **50** : 3826–3851. DOI: 10.1002/ 2013WR014227

Dankers R, Feyen L. 2009. Flood hazard in Europe in an ensemble of regional climate scenarios. Journal of Geophysical Research: Atmospheres **114** : 47–62. DOI: 10.1029/2008JD011523

Demarchi L, Bizzi S, Piegay H. 2017. Regional hydromorphological characterization with continuous and automated remote sensing analysis based on VHR imagery and low-resolution LiDAR data. ESPL **42** : 531–551. DOI: 10.1002/esp.4092

Detert M, Weitbrecht V. 2013. User guide to gravelometric image analysis by BASEGRAIN. Advances in Science and Research – Fukuoka et al. (2013) : 1789–1795.

Downs PW, Dusterhoff SR, Leverich GT, Soar PJ, Napolitano MB. 2018. Fluvial system dynamics derived from distributed sediment budgets: perspectives from an uncertainty-bounded application. Earth Surface Processes and Landforms **43** : 1335–1354. DOI: 10.1002/esp.4319

Eaton BC, Millar RG, Davidson S. 2010. Channel patterns: Braided, anabranching, and single-thread. Geomorphology **120** : 353–364. DOI: 10.1016/j.geomorph.2010.04.010

Fehr R. 1987. Einfache Bestimmung der korngrös-senverteilung von Geschiebematerial mit Hilfe der Linienzahlanalyse (Simple detection of grain size distribution of sediment material using line-count analysis). Schweizer Ingenieur und Architekt **105(38)** : 1104–1109.

Ferguson RI, Church M, Rennie CD, Venditti JG. 2015. Reconstructing a sediment pulse: Modeling the effect of placer mining on Fraser River, Canada. Journal of Geophysical Research: Earth Surface **120** : 1436–1454. DOI: 10.1002/2015JF003491

Forzieri G, Feyen L, Rojas R, Flörke M, Wimmer F, Bianchi A. 2014. Ensemble projections of future streamflow droughts in Europe. Hydrol. Earth Syst. Sci. **18** : 85–108. DOI: 10.5194/hess-18-85-2014

Fouache E, Gruda G, Mucaj S, Nikolli P. 2001. Recent geomorphological evolution of the deltas of the rivers Seman and Vjosa, Albania. Earth Surface Processes and Landforms **26** : 793–802. DOI: 10.1002/esp.222

Fredsøe J. 1978. Meandering and braiding of rivers. Journal of Fluid Mechanics **84** : 609–624. DOI: 10.1017/S0022112078000373

Fryirs K. 2013. (Dis)Connectivity in catchment sediment cascades: a fresh look at the sediment delivery problem. Earth Surface Processes and Landforms **38** : 30–46. DOI: 10.1002/esp.3242

Fryirs KA. 2017. River sensitivity: a lost foundation concept in fluvial geomorphology. Earth Surface Processes and Landforms **42** : 55–70. DOI: 10.1002/esp.3940

Fryirs KA, Wheaton JM, Bizzi S, Williams R, Brierley GJ. 2019. To plug-in or not to plug-in? Geomorphic analysis of rivers using the River Styles Framework in an era of big data acquisition and automation. WIREs Water **6** : e1372. DOI: 10.1002/wat2.1372

Gilbert JT, Wilcox AC. 2020. Sediment Routing and Floodplain Exchange (SeRFE): A Spatially Explicit Model of Sediment Balance and Connectivity Through River Networks. Journal of Advances in Modeling Earth Systems **12** : e2020MS002048. DOI: 10.1029/2020MS002048

Heckmann T, Schwanghart W. 2013. Geomorphic coupling and sediment connectivity in an alpine catchment - Exploring sediment cascades using graph theory. Geomorphology **182** : 89–103. DOI: 10.1016/j.geomorph.2012.10.033

Hohensinner S, Egger G, Muhar S, Vaudor L, Piégay H. 2021. What remains today of pre-industrial Alpine rivers? Census of historical and current channel patterns in the Alps. River Research and Applications **37** : 128–149. DOI: https://doi.org/10.1002/rra.3751

Knighton AD. 1998. Fluvial Forms and Processes. A New Perspective . Arnold: London

Kondolf G. 1997. PROFILE: Hungry Water: Effects of Dams and Gravel Mining on River Channels. Environmental management **21** : 533–51.

Kondolf GM, Montgomery DR, Piegay H, Schmitt L. 2003. Geomorphic classification of rivers and streams. In Tools in fluvial geomorphology , Kondolf GM and Piegay H (eds). Chichester; 169–202.

Leopold LB, Wolman MG. 1957. River channel patterns - braided, meandering, and straight. US Geological Survey Professional Paper 282(B) : 39–85.

Liébault F. 2003. Les rivières torrentielles des montagnes drômoises : évolution contemporaine et fonctionnement géomorphologique actuel (massifs du Diois et des Baronnies), thesis, Lyon 2, 1 January [online] Available from: http://www.theses.fr/2003LYO20067 (Accessed 30 January 2020)

Liébault F, Piegay H. 2001. Assessment of channel changes due to long term bedload supply decrease, Roubion River, France. Geomorphology **36** : 167–186.

Lugo GAG, Bertoldi W, Henshaw AJ, Gurnell AM. 2015. The effect of lateral confinement on gravel bed river morphology. Water Resources Research **51** : 7145–7158. DOI: https://doi.org/10.1002/2015WR017081

Millar RG. 2005. Theoretical regime equations for mobile gravel-bed rivers with stable banks. Geomorphology **64** : 207–220. DOI: 10.1016/j.geomorph.2004.07.001

Milliman J, Farnsworth K. 2011. Runoff, erosion, and delivery to the coastal ocean . Cambridge University Press.

Mueller ER, Pitlick J. 2014. Sediment supply and channel morphology in mountain river systems: 2. Single thread to braided transitions. Journal of Geophysical Research: Earth Surface **119** : 1516–1541. DOI: 10.1002/2013JF003045

Parker G, Klingeman PC. 1982. On why gravel bed streams are paved. Water Resources Research **18** : 1409–1423. DOI: 10.1029/WR018i005p01409

Peters R, Berlekamp J, Lucía A, Stefani V, Tockner K, Zarfl C. 2021. Integrated Impact Assessment for Sustainable Hydropower Planning in the Vjosa Catchment (Greece, Albania). Sustainability **13** : 1514. DOI: 10.3390/su13031514

Piégay H, Alber A, Slater L, Bourdin L. 2009. Census and typology of braided rivers in the French Alps. Aquatic Sciences Research Across Boundaries **71** : 371–388. DOI: 10.1007/s00027-009-9220-4

Reid HE, Brierley GJ. 2015. Assessing geomorphic sensitivity in relation to river capacity for adjustment. Geomorphology **251** : 108–121. DOI: http://dx.doi.org/10.1016/j.geomorph.2015.09.009

Rizzoli P et al. 2017. Generation and performance assessment of the global TanDEM-X digital elevation model. ISPRS Journal of Photogrammetry and Remote Sensing **132** : 119–139. DOI: 10.1016/j.isprsjprs.2017.08.008

Roux C, Alber A, Bertrand M, Vaudor L, Piégay H. 2015. “FluvialCorridor”: A new ArcGIS toolbox package for multiscale riverscape exploration. Geomorphology **242** : 29–37. DOI: 10.1016/j.geomorph.2014.04.018

Schiemer F, Drescher A, Hauer C, Schwarz U. 2018. The Vjosa River corridor: a riverine ecosystem of European significance. **155** : 1–40. DOI: https://doi.org/10.1007/s10980-020-00993-y

Schmitt R, Bizzi S, Castelletti A. 2016. Tracking multiple sediment cascades at the river network scale identifies controls and emerging patterns of sediment connectivity. Water Resources Research **52** : 3941–3965. DOI: 10.1002/2015WR018097

Schmitt R, Bizzi S, Castelletti A. F., Kondolf G. M. 2017. Stochastic Modeling of Sediment Connectivity for Reconstructing Sand Fluxes and Origins in the Unmonitored Se Kong, Se San, and Sre Pok Tributaries of the Mekong River. Journal of Geophysical Research: Earth Surface **123** : 2–25. DOI: 10.1002/2016JF004105

Schmitt R, Bizzi S, Castelletti A, Kondolf GM. 2018. Improved trade-offs of hydropower and sand connectivity by strategic dam planning in the Mekong. Nature Sustainability **1** : 96. DOI: 10.1038/s41893-018-0022-3

Schmitt RJP, Bizzi S, Castelletti A, Opperman JJ, Kondolf GM. 2019. Planning dam portfolios for low sediment trapping shows limits for sustainable hydropower in the Mekong. Science Advances **5** : eaaw2175. DOI: 10.1126/sciadv.aaw2175

Schumm SA. 1985. Patterns of alluvial rivers. Annual review of earth and planetary sciences **13** : 5–27.

Schwanghart W, Kuhn NJ. 2010. TopoToolbox: A set of Matlab functions for topographic analysis. Environmental Modelling & Software **25** : 770–781. DOI: 10.1016/j.envsoft.2009.12.002

Shih S-M, Komar PD. 1990. Differential bedload transport rates in a gravel-bed stream: A grain-size distribution approach. Earth Surface Processes and Landforms **15** : 539–552. DOI: 10.1002/esp.3290150606

Surian N, Rinaldi M. 2003. Morphological response to river engineering and management in alluvial channels in Italy. Geomorphology **50** : 307–326. DOI: https://doi.org/10.1016/S0169-555X(02)00219-2

Tangi M, Schmitt R, Bizzi S, Castelletti A. 2019. The CASCADE toolbox for analyzing river sediment connectivity and management. Environmental Modelling & Software **119** : 400–406. DOI: 10.1016/j.envsoft.2019.07.008

Van Der Knijff JM, Younis J, De Roo a. PJ. 2010. LISFLOOD: a GIS-based distributed model for river basin scale water balance and flood simulation. International Journal of Geographical Information Science **24** : 189–212. DOI: 10.1080/13658810802549154

Wessel B. 2018. TanDEM-X Ground Segment – DEM Products Specification Document [online] Available from: https://tandemx-science.dlr.de/ (Accessed 30 January 2020)

Wohl E et al. 2018. Connectivity as an emergent property of geomorphic systems. Earth Surface Processes and Landforms **0** DOI: 10.1002/esp.4434 [online] Available from: https://onlinelibrary.wiley.com/doi/abs/10.1002/esp.4434